# A Numerical Approach for Simulating a High-Speed Train Passing through a Tornado-Like Vortex

R. Z. Xu[1], F. Wu[2†], W. H. Su[3], J. F. Ding[4] and D. Vainchtein[5]

[1]*Key Laboratory of Traffic Safety on Track, Ministry of Education, School of Traffic & Transportation Engineering,Central South University, Changsha 410075, Hunan, China*
[2] *Joint International Research Laboratory of Key Technologies for Rail Traffic Safety, Changsha 410075, Hunan, China*
[3] *National & Local Joint Engineering Research Center of Safety Technology for Rail Vehicle, Changsha 410075, Hunan, China*
[4] *Department of Applied Mathematics, University of Waterloo, Ontario N2L3G1, Canada*
[5] *Nyheim Plasma Institute, Drexel University, Camden, NJ, USA*

† *Corresponding Author Email: gszxcfd wf@csu.edu.cn*

## ABSTRACT

Tornados are one of the most common natural disasters, but their occurrence can be sudden and unpredictable. For trains operating in the areas where tornadoes frequently happen, the operation safety is challenged. Tornado generator was recently proposed as a method of numerical investigation of tornado-like vortex flows. This paper presents a numerical approach for the simulation of train passing through a tornado-like vortex on realistic scale. It is found that the tornado-like vortex causes appearance of localized regions of a negative pressure on the train and transient variations of the aerodynamic loads acting on the train. As a result, the tornado-like vortex causes swings on the lateral force, and subsequently on the rolling moment, which affect the passenger comfort and operation safety of the train. The method presented herein can be further applied to the study of train behavior and real time response while encountering tornadoes of different types and strength, which is significant for evaluating the operation safety of high-speed trains.

**Keywords**: Tornado-like vortex; High-speed train; Train aerodynamic; Fluid-solid interaction; Train safety.

## NOMENCLATURE

| | | | |
|---|---|---|---|
| $C_1$ | head car | $r$ | radial coordinate |
| $C_2$ | middle car | $R_{max}$ | core radius of tornado |
| $C_3$ | tail car | $S$ | swirl ratio of tornado |
| $C_{Mx}$ | coefficient of rolling moment | $S_A$ | characteristic area of the train |
| $C_y$ | coefficient of lateral force | $t$ | time variable |
| $C_z$ | coefficient of lift force | $\vec{t}$ | unit tangential |
| $d^0, d^-, d^+$ | train operation paths | $U_\theta$ | tangential velocity |
| $F_y$ | lateral force | $U_{\theta,max}$ | maximum tangential velocity |
| $F_z$ | lift force | $V$ | characteristic velocity |
| $g$ | gravity | $W$ | width of the train |
| $H$ | characteristic height of the train | $y+$ | wall y-plus |
| $m$ | mass of the train | | |
| $\vec{n}$ | unit normal | $\theta$ | orientation of the guide vanes |
| $M_x$ | rolling moment | $\rho$ | air density |
| $p$ | pressure | $\tau$ | shear stress |
| $Q$ | volumetric flow rate | | |

## 1. INTRODUCTION

Rapid development of high-speed rail requires the assurance of the operational safety and passenger comfort of trains under extreme conditions, as trains run through various, rapidly changing environments. Tornado is a common natural disaster, characterized by a sudden occurrence, relatively short duration,

and unpredictable path. All these features make tornados rather difficult to accurately forecast. It causes localized but strong damage and may inflict significant economic losses and casualties every year Ashley (2007), Simmons and Sutter (2008). A train was overturned by a tornado in Japan as reported in Suzuki and Okura (2016). Frequent appearances of tornadoes near the east coast of China threaten the operational safety of high-speed trains running through this area Xu *et al.*(2013). Thus, it is important to investigate the interaction of a tornado and a high-speed train and to determine the potential risks to the train's safety.

Extensive experimental, numerical, and theoretical research has been conducted to understand the formation mechanism and flow characteristics of natural tornadoes. Alexander and Wurman (2004), Wurman and Alexander (2004), Wurman *et al.*(2013) measured the tangential velocity distribution of a natural tornado at different heights with the Doppler radar. However, it is quite risky to obtain data from natural tornadoes, and individual tornado vary significantly in their characteristics, which makes laboratory experiments and numerical simulations the most popular approaches. Experimentally, the tornado generator is usually applied to produce a tornado-like swirling flow (tornado-like vortex). Ward (1972) designed a stationary tornado-like vortex using an axial fan on the top to generate the updraft, guide vanes near the floor to provide the angular momentum for the rotational flow, and a honeycomb panel to remove the vertical vorticity. The Haan's group experimentally produced a marching tornado along a suspended track of about 10 meters in length to study the down-burst of tornado Haan *et al.* (2008). In recent years, the particle image velocimetry (PIV) technique has been adopted to visualize the flow field and to quantitatively study the velocity distribution in tornadoes. Tari *et al.* (2010), Refan and Hangan (2018) used PIV to determine the velocity field of tornado-like vortices over a broad range of swirling strength. Numerically, the tornado-like vortex can be obtained by simulating the laboratory tornado generators. The large eddy simulation (LES) is an efficient and precise approach for the numerical reconstruction of tornado-like vortex Ishihara *et al.* (2011), Natarajan and Hangan (2012), Liu and Ishihara (2015), Liu *et al.* (2018a), Liu *et al.* (2018b). Additionally, the axial symmetry of the tornado flow field allows the application of theoretical analysis. Starting with Burgers (1948), a series of mathematical models are proposed to describe the flow characteristics of tornadoes Winn *et al.* (1999), Mishra *et al.* (2008), Bech *et al.* (2009), Tari *et al.* (2010), Kosiba and Wurman (2010), Wood and Brown (2011), Refan and Hangan (2016), Tang *et al.* (2018), Baker and Sterling (2017), Baker and Sterling (2018b).

In terms of the operational safety of high-speed trains, the recent research mainly focuses on the train running through crosswind. Suzuki *et al.*(2003) used three kinds of wind tunnel tests to evaluate the aerodynamic characteristics of the vehicles with different ground configurations, such as bridges and embankments. Eichinger *et al.* (2015), Zhuang and Lu (2015) used the trainsient numerical methods (e.g. Detached Eddy Simulation and Large Eddy Simulation) to explore the aerodynamic characteristics of high-speed trains under crosswinds. Chen *et al.* (2018) investigated the influence of strong crosswind on the aerodynamic performances of four trains with different streamlined lengths using DES.

Recently, the interaction of moving vehicles and tornado-like vortices was investigated experimentally and theoretically. Suzuki and Okura (2016), Suzuki *et al.* (2016) designed a movable tornado generator to create a double vortex in front of a moving train to measure the pressure distribution on the train moving through the vortices. The lateral force, lift, and overturning moment can be calculated from the experimental data. Paulikas *et al.* (2016) recorded the real-time behavior of a stationary vehicle residing near by a realistic tornado. The measured results may serve as a basis for better operational safety protocols, and for designing safer vehicles and infrastructures. Haan *et al.* (2017) derived a relationship between the critical speed for vehicle safety and the tornado wind speed through experimental measurements. Baker and Sterling (2018a) further improved a theoretical method to predict the potential risk of train over-turning with the presence of tornadoes based on their previously established tornado model Baker and Sterling (2017). However, research on the interaction of trains and tornado-like vortices has just been initiated, and is still wide open.

In the present study, we establish a new numerical approach to study what happens when a high-speed train runs through a tornado-like vortex. We built the vortex using a tornado generator and compared the flow field with existing mathematical models. We simulated the motion of the train by the sliding mesh technique, and validated it with the moving model test. We computed aerodynamic forces acting on the train running through the vortex along three distinct paths. We conclude with comparing our results with existing studies and discussing the immediate consequences to the operational safety of the trains.

## 2. PROBLEM SETUP

### 2.1 Tornado air flow and Classification of Tornadoes

A typical tornado is funnel-shaped fluid structure. Almost all the tornadoes in the Northern Hemisphere rotate counter-clockwise. Its velocity has three components: tangential, radial, and vertical, with tangential velocity being significantly larger than the other two. The maximum magnitude of the tangential velocity defines the intensity of a tornado, which is characterized by the enhanced Fujita (EF) scale, from EF0 to EF5, with EF5 being the strongest, McDonald *et al.* (2006), Paulikas *et al.* (2016). The occurrence rate drops rapidly as the intensity level increases: about 70% of all observed and recorded tornadoes are EF0 or EF1 Charles *et al.* (2009), Xue *et al.* (2016). In this study, we considered a tornado-

like vortex equivalent to the intensity of EF1, whose maximum velocity is between 39 and 49m/s and the width between 15 and 60 meters. The paths of tornadoes are typically quite short (typically under 6km for EF0 or EF1) and unpredictable.

## 2.2 Layout of the Train Moving Through the Vortex

In realistic settings, both train and tornado move. And although a speed of tornado's propagation can reach 100km/h, a typical tornado travels at $10 - 30$km/h NOAA (2018). While this speed is important and must be taken into consideration when studying the tornado-structure interaction, this speed is much smaller than characteristic speeds of high-speed trains, which are about $200 - 400$km/h. In this sense, for the purpose of the present study, it is reasonable to assume that the tornado is stationary.

Effects of tornado on the train clearly depends on the distance between the path of the train and the center of the tornado. Tornados almost always propagate on the plains, and the rail tracks are usually straight there. In the present study we considered the train moving along one of three straight paths: through the center or on either side of the vortex. As shown in Fig. 1, these paths are along the x-axis and are 5m apart. Let $d^0$ denote the case when the train runs through the center of the vortex, while $d^+$ and $d^-$ are to the left and right of $d^0$, respectively. Major difference between the three cases is the relationship between the direction of local air flow and train motion. The train moves essentially against the rotating air flow on $d^+$, perpendicular to it on $d^0$, and along it on $d^-$, which results in significantly different flow characteristics and resultant forces.
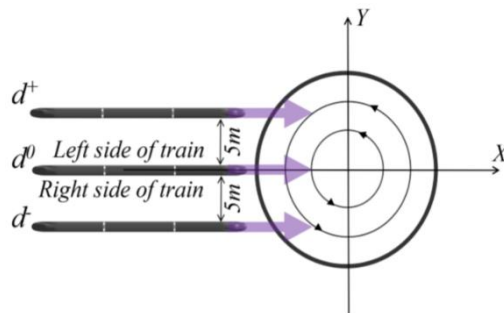


**Fig. 1. Schematic of train running through the tornado-like vortex (top view).**

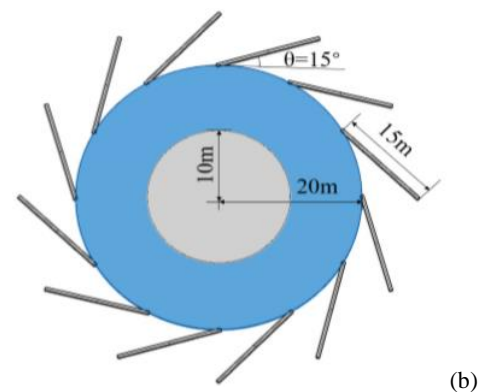## 3. NUMERICAL GENERATOR OF TORNADO-LIKE VORTEX

### 3.1 Geometry of the Generator and the flow of Tornado-like Vortex

The formation mechanism and the structure of tornado is complicated. To obtain the flow field of a tornado numerically, we developed an artificial tornado generator based on the ones proposed in Ishihara *et al.* (2011), Liu and Ishihara (2015). Main difference between the generator in the present paper and the published setups is the height, arrangement, and modifications of the guide vanes required for the

train to pass through. The generator has three parts: the inflow region (blue cylinder), the outflow region, and the guide vanes (Fig. 2). Essentially, the generator consists of two cylinders: the larger, inflow, is at the bottom, and the smaller, out-flow, is at the top. The sides of the outflow region and the top ring of the inflow region are solid walls. Note, that the cylinders and the vanes are stationary. The air flow is created by the pressure gradient. The outflow region works as an air pump and sucks the air out from the generator chamber. Twelve stationary guide vanes are equally spaced and attached to the inflow region. The air flows into the inflow region through the gaps between the guide vanes. The vanes are oriented in such a way that the air spins counter-clockwise in the inflow region and forms a tornado-like vortex in the inflow region. Dimensions of the generator, as shown in Fig. 2, were chosen so that the width of the inflow region (20m in radius) matches the characteristic width of a typical tornado, and the height of the inflow region (20m) is much larger than the height of the train (under 4m). The numerical vortex generated by this approach is stationary, but possesses distributions of tangential velocity and pressure similar to realistic tornadoes.
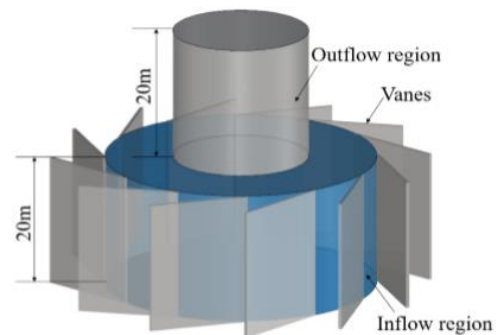


(a) Perspective view



Top view

**Fig. 2. Model of tornado-like vortex generator.**

Let $\theta$ be the angle between vanes and the tangential direction of the inflow region at the contact positions, see Fig. 2(b). The strength of the tornado-like vortex depends on the (negative) gage pressure at the top of the outflow region and the value of $\theta$. Large negative gage pressure and small $\theta$ angles result in a stronger vortex. We chose $\theta = 15°$ to match the strength of

EF1 tornado. Once θ is set, the strength of the numerical tornado can be further adjusted by varying the pressure. In our model the pressure was set to −2000Pa.

The velocity and pressure distributions of the vortex generator are shown in Fig. 3. The flow field possesses the basic features of a tornado. Streamlines in Fig. 3(a) show that the flow inside the inflow region is highly rotational and nearly axisymmetric. A 'tornado eye' (a low pressure region) is in the center of the tornado-like vortex, see Fig. 3(b). The pressure increases rapidly with the distance from the eye. Although the structure of numerical vortex does not resemble a tornado near the pressure out-let (the top of panel (b)), the height of the reliable region of the tornado-like vortex (roughly 20m) is sufficient to study the train-vortex interaction as the total height of the train is less than 4m.



(a)



(b)
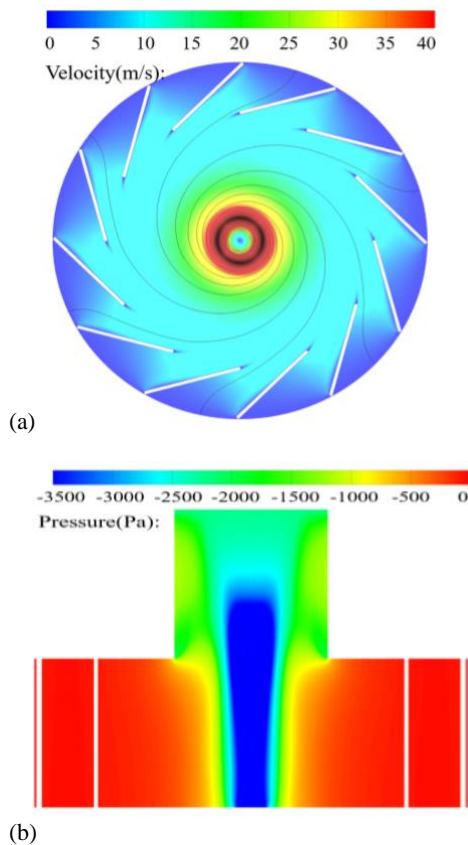
**Fig. 3. Flow structure and pressure of the tornado-like vortex. (a) Velocity distribution in the inflow region on the horizontal plane 2.28m above the ground. Black curves are streamlines, (b) Pressure distribution on the vertical plane of the tornado generator.**

## 3.2. Adjustment to the Generator for a Train to Pass

One can see from Fig. 2, that the guide vanes leave no room for the train to pass. Thus we modified the numerical tornado generator as shown in Fig. 4: we created a 'hole' by partially removing the guide vanes. The hole is rectangular when looked along the moving train. It is 8.6m wide and 6.0m high. We

chose those dimensions according to three criteria: (a) the hole must be large enough to let the train pass through, (b) the hole should not significantly affect the formation of the vortex compared with the original setup, (c) pressure fluctuations induced by vanes on the train should be small comparing to that induced by the vortex. Criteria (c) will be verified in Sect. 6. A modified tornado generator is created for each of the three paths described above, $d^+$, $d^0$, and $d^-$. Although size of the hole is identical for all three generators, the geometric models slightly differ due to the orientation of guide vanes.



(a) View in the direction of train operation



(b) Perspective view
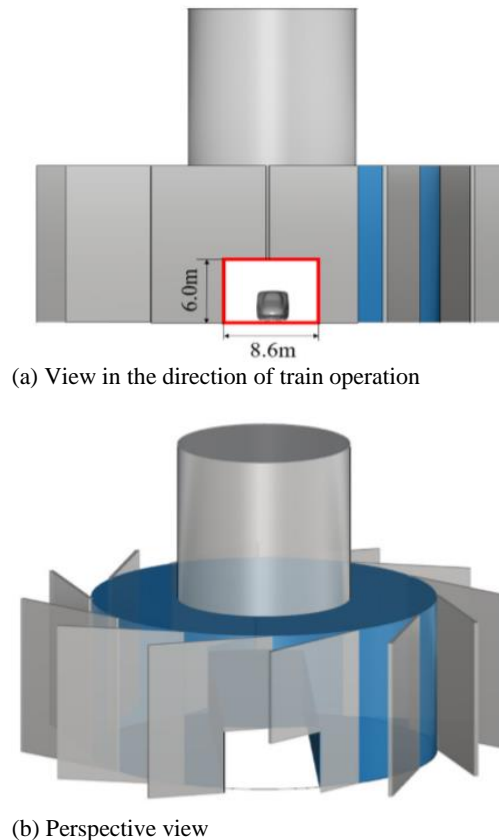
**Fig. 4. Modified model of the tornado-like vortex generator for d0 case.**

## 3.3 Verification of the Generator with and Without the Hole

First, we need to verify that the radial distribution of the tangential velocity in the generator matches the matches standard approximations of a tornado. The Burgers-Rott vortex model is a widely used theoretical approximation for the tangential velocity, $U_\theta(r)$, of a tornado-like vortex Burgers (1948), Wood and Brown (2011):

$$U_\theta(r) = \frac{A}{r}(1 - \exp(-Br^2)) \qquad (1)$$

where r is the radial distance from the 'tornado eye', and $A$ and $B$ are model parameters. Let $U_{\theta,max}$ be the maximum magnitude of tangential velocity for a given tornado-like vortex, and $R_{max}$ be the radial distance where $U_\theta = U_{\theta,max}$. $R_{max}$ is called the core radius of a tornado. Comparison of the numerical

tornado-like vortices and the Burgers-Rott vortex, Eq. (1), is presented in Fig. 5. The numerical tornado-like vortices are generated for the $d^0$, $d^+$, and the unmodified generators. The vortex for $d^-$ is not shown as the generator is identical to the $d^+$ case rotated by 180°. For each setting, velocity and the distance are normalized by $U_{\theta,max}$ and by $R_{max}$ for that particular setting, respectively. Both unmodified and modified generators are in a good agreement with the theoretical model. The hole in the generators barely affects the flow structure of the tornado-like vortices. Note that the tangential velocity of the Burgers-Rott model goes to 0 at the vortex center. However, that of the numerical vortices at the origin is non-zero, due to the finite computational mesh. It can be improved by higher resolution and does not significantly affect the simulations.
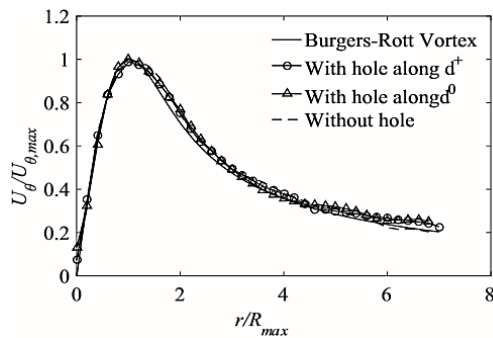


**Fig. 5. Normalized tangential velocity for tornado-like vortices compared with the Burgers-Rott vortex.**

A dimensionless parameter that defines the structure of a tornado-like vortex is the swirl ratio S, which is essentially the ratio of the angular momentum and the vertical momentum, see Church *et al.*(1979):

$$S = \pi R_{max}^2 U_{\theta,max}/Q \qquad (2)$$

where $Q$ is the volumetric flow rate through the pressure outlet. The vortex is single-cell for $S <0.5$, and multi-cell otherwise Haan *et al.* (2008). In our simulations, $Q \approx 10^4 m^3/s$.

The values of $R_{max}$, $U_{\theta,max}$, and $S$ of the numerical tornado-like vortices are presented in Table 1. The parameters of the vortices produced numerically by the generators with or without the hole are in a good agreement. Thus, the validation confirms that all the considered tornado-like vortices are quite similar in terms of their structure and intensity, and all of them resemble the Burgers-Rott vortex model.

**Table 1 Parameters of the numerical tornado-like vortices**

| Generator | $R_{max}$ (m) | $U_{\theta,max}$ (m · s$^{-1}$) | S |
|---|---|---|---|
| Without hole | 2.71 | 40.75 | 0.0920 |
| With hole along d0 | 2.63 | 41.08 | 0.0901 |
| With hole along d$^+$ or d$^-$ | 2.66 | 40.60 | 0.0909 |

## 4. TRAIN MODEL AND DYNAMICS

### 4.1 Train Geometry

In this paper we investigate the aerodynamic interaction between a moving train and a stationary tornado-like vortex. The high-speed train considered in this study consists of 3 cars, see Fig. 6. The same train model has been widely used in other studies on high-speed trains Huang *et al.* (2014), Liu *et al.* (2017), Niu *et al.* (2018). The head, middle, and tail car are called $C_1$, $C_2$, and $C_3$, respectively. The cars $C_1$ and $C_3$ are identical, with $C_3$ facing backward. For the convenience of numerical discretization, the surface of the train was smoothed out, and the geometries of the bodies and the connections between cars were simplified.



(a) Front view



(b) Side view
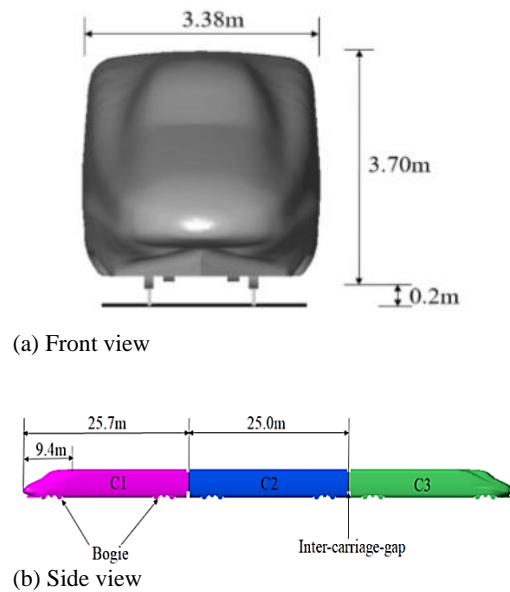
**Fig. 6. Train model used in numerical simulations.**

To illustrate pressure fluctuations on the train surface, we selected several pairs of monitoring points. Each pair of points is symmetric with respect to the middle (longwise) plane of the train. Figure 7 shows the locations of monitoring points on $C_1$. Points 1, 2, and 3 are on the left side of the train looking forward, while points 4, 5, and 6 are on the right side. Point 1 is directly opposite to point 4 and so on. We denote the $j$ −th monitoring point on the $i$ −th car as $P_i − j$.
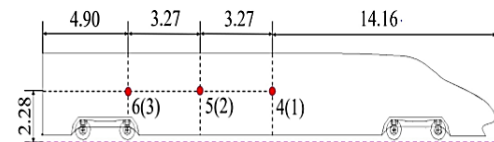


**Fig. 7. Monitoring points (red dots) on the surface of car C1. Notation 4(1) indicates that point 1 is on the other side of the train directly opposite to point 4. All the lengths are in meters.**

## 4.2 Train's Motion

At *t = 0*, the tornado generator functions normally to produce a tornado-like vortex inside it. The train is 113m away from the center of the vortex and starts moving along one of the three paths at 250km/h ≈ 70m/s. The computation ends when the tail end leaves the tornado generator.

The train's progress is illustrated in Fig. 8. The grey color represents the tornado-like vortex, and the red color indicates the vortex core. For example, at *t = 2s*, the head of the train is about 36m past the vortex center, and the tail end of the train is about 40m before it. The head of train reaches the vortex region at *t = 1.34s*, and the tail end leaves the vortex region at *t = 3.01s*.
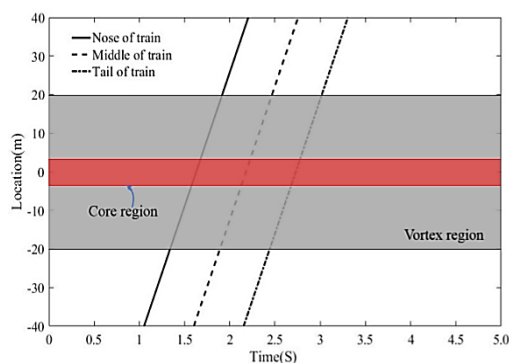


**Fig. 8. Position of train nose, middle, and tail as a function of time. The grey and red color indicate the region of the tornado-like vortex, and the vortex core, respectively.**

## 5. NUMERICAL MODEL AND SETUP

### 5.1 Numerical algorithm for flow simulation

In this study, the numerical simulations are performed using ANSYS Fluent, which is a finite volume method based solver for the Navier-Stokes equations. The speed of the train is 250km/h. Simulations are conducted on the real (1:1) scale. The flow Reynolds Number is high, about 106, and the Mach Number is less than 0.3. Thus the flow can be considered to be incompressible, but intensively turbulent. The numerical semi-implicit method for pressure-linked equations consistent (SIMPLEC) scheme is adopted for solving the in-compressible Navier-Stokes equations Wang *et al.* (2019). The unsteady Reynolds Averaged Navier-Stokes (URANS) turbulence models are usually applied for the computation of turbulent flow induced by train motion Wang *et al.* (2018), Zhang *et al.* (2017a), as the consumption of computational re-source required by URANS is acceptable for simulating train motion. In the current study, the unsteady $k - \varepsilon$ RNG turbulence model with a standard wall function is chosen for simulations as it possesses relatively higher precision for rotational flows. The k and ε equations are discretized with a second-order upwind scheme. The simulation is performed with a time interval of $\Delta t = 10^{-3}$s. Similar to Li *et al.* (2017), Zhang *et al.* (2017b), Li *et al.* (2019a), numerical solution of each time step is considered to be converged when all the residuals are simultaneously less than $10^{-4}$.

## 5.2 Computational Domains and Boundary Conditions

The computational domain and boundary conditions are shown in Fig. 9. The tornado generator is located at the center of a rectangular domain, which is 400m long, 100m wide, and 20m high. The height of the domain is equal to height of the inflow region and the guide vanes. The four sides and the upper boundaries are set as pressure inlets with ambient pressure (0Pa). The bottom of the domain and the sides of outflow cylinder are non-slip walls. The upper boundary of the outflow region is a pressure outlet, which is set to a constant negative pressure. For the EF1 tornado strength, the pressure at the pressure outlet = −2000Pa (see Sect.3). The air flow, driven by the pressure outlet, enters the computational domain from the pressure inlets, passes through the gaps between the guide vanes, circulates inside the inflow region, and leaves from the pressure outlet.
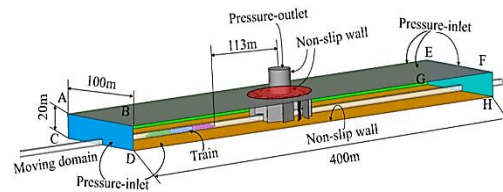


**Fig. 9. Schematic of the computational domain and boundary conditions.**

The sliding mesh technique is used to address the train motion. The entire computational domain is divided into two separate regions. The region that contains the train is a moving region with a translational velocity being the operating speed of the train, and rest of the domain is a stationary region. The flow field information, such as velocity and pressure, is exchanged between the moving and stationary domains.

### 5.3 Mesh

The numerical configuration of the current study is somewhat similar to the scenario of train passing through a tunnel, except that the tunnel is replaced by a tornado generator and a tornado-like vortex. For these cases, a large amount of computational resource is required to simulate transient processes, even when using the sliding mesh technique. The hybrid mesh is applied to the numerical simulations of these scenarios, and both the computational precision and efficiency are acceptable for engineering computations Wang *et al.* (2018), Li *et al.* (2019b). The bogie area under the train and the connection gap between each car are discretized with unstructured mesh, while everywhere else including the moving and stationary domains is discretized with structured mesh, as shown in Fig. 10.
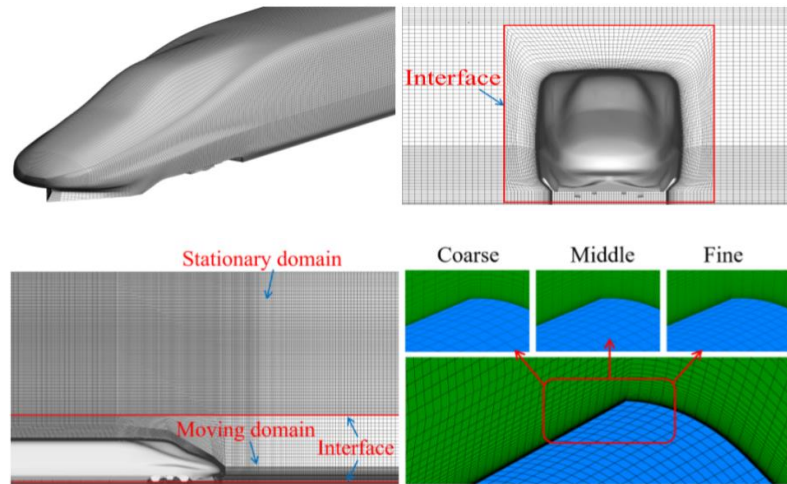
**Fig. 10. Hybrid mesh for numerical computation: unstructured in the bogie area, and structured everywhere else. (a) surface mesh on C1; (b) front view; (c) side view; (d) Mesh with different sizes for sensitivity test, where blue is the train surface mesh and green is the space mesh.**

**Table 2 To check that the numerical solutions are stable for. Mesh information for different mesh sizes**

| Mesh | Average surface mesh size (mm) | First layer thickness (mm) | Growth ratio | Total cells (million) |
|---|---|---|---|---|
| Coarse | 60 | 0.8 | 1.02 | 38 |
| Medium | 50 | 0.8 | 1.05 | 43 |
| Fine | 40 | 0.8 | 1.08 | 51 |
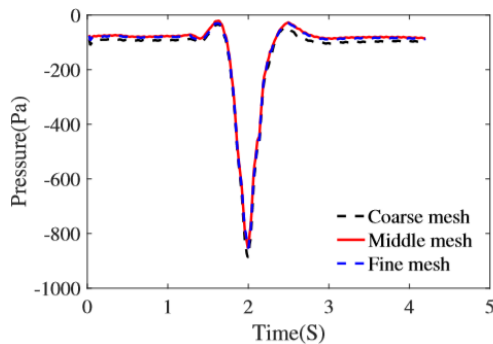


(a) Monitoring point $P_1$-1
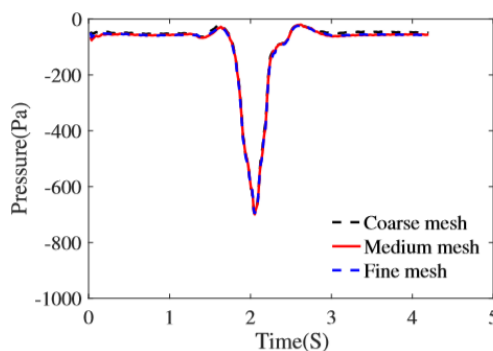


(b) Monitoring point $P_1$-2

**Fig. 11. Comparison of pressure fluctuation for train passing through the tornado-like vortex along $d^0$ at 250km/h for different mesh sizes.**

To check that the numerical solutions are stable for different mesh densities, three sets of mesh were generated, namely called the coarse, medium, and fine mesh, with averaged mesh size on the train surface being 60mm, 50mm, and 40mm, respectively. The spatial mesh near the train surface was refined to meet the requirement of wall y+ of the selected $k - \varepsilon$ turbulence model. Note that the thickness of the first layer mesh is identical for all the mesh sizes to ensure that the wall y+ on the train surface is not affected. Detailed information of the mesh sets are listed in Table 2.

Numerical simulations for the train running through the tornado-like vortex along d0 at 250km/h, were performed using the coarse, medium, and fine mesh. Pressure variations at points $P_1 - 1$ and $P_1 - 2$ are presented in Fig. 11. The results for the medium and fine meshes are nearly identical, while that of the coarse mesh slightly differs from the other two. which indicates that the numerical tornado generated, as well as the process of train running through the tornado, are nearly identical for the medium and fine mesh cases.

The distribution of wall y+ on the train surface at 250km/h before the train reaches the tornado region is shown in Fig. 12. As the thickness of the first layer mesh is identical to all mesh sizes (0.8mm), only the y+ distribution for the medium mesh is demonstrated. One can see that the wall y+ on most of the train surface is around 100 or less, which satisfies the corresponding requirement of the $k - \varepsilon$ turbulence model. Large y+ value (around 200) appears in the locations where unstructured mesh is applied, due to a relatively coarse mesh refinement there. Considering both the tested pressure variations and wall y+ distribution, the medium mesh was adopted for the numerical study hereafter.
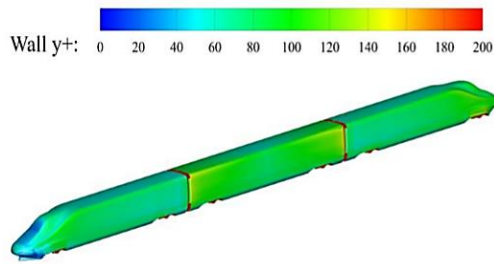
**Fig. 12. Distribution of y+ value on the train surface during operation in open air at 250km/h.**

## 6. VALIDATION OF THE NUMERICAL METHOD

To verify the validity of the numerical setup, we checked (i) the precision of sliding mesh method for the computation of pressure on the train surface, and (ii) pressure variations on the train induced just by the walls and vanes of the tornado generator, without the tornado air flow.

### 6.1 Validation of the Sliding Mesh Method

To test the numerical accuracy of the sliding mesh method used in this study, a test was performed with the train running in open air on the moving model test platform at Central South University, China (Fig. 13). The test was conducted on the 1 : 20 scale with an operating speed of 250km/h using a train model identical to the numerical simulation described above. Eighteen differential pressure sensors were positioned on both sides of the train matching the locations of the monitoring points in the numerical simulations (see Sect. 4.1). The C1 multi-channel recording system (IMC, Inc) was used for pressure data acquisition and storage. The data was collected at 1kHz sampling frequency and high-pass filtered ($250\ Hz$) to remove the fluctuations caused by mechanical vibrations. The test was repeated 5 times to ensure the consistency of test results.



**Fig. 13. Picture of moving model experimental test.**

A train running in open air at a constant speed is a quasi-steady process, and pressure on the train surfaces remains nearly constant. The unstreamlined part of the train has a slightly negative pressure. Data from two pressure sensors on $C_1$, averaged over 5 runs, is presented in Fig. 14. As the experiment is conducted with 1 : 20 scale, the experimental time scale in Fig. 14 is converted to the real scale (1 : 1) by multiplying the experimental time by 20. The pressure at points $P_1-2$ and $P_1-5$ are roughly $-50$Pa and relatively stable. The pressure behavior of other sensors is similar. The numerical results are in a good agreement with the experimental data, which validates the numerical method of simulating train's motion.
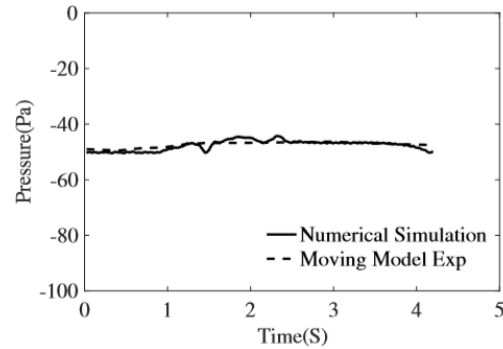


(a) Monitoring point $P_1$-2
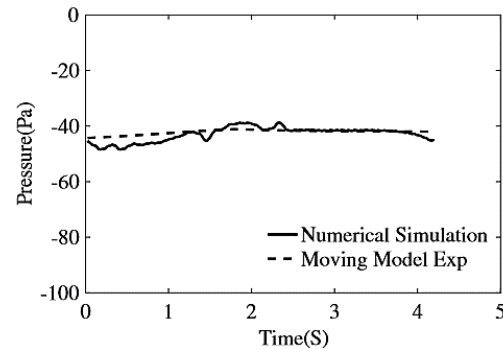


(b) Monitoring point $P_1$-5

**Fig. 14. Comparison of pressure fluctuations between a moving model test train and a numerical simulation. The train ran in the open air, without the tornado generator or the tornado-like vortex.**

### 6.2 Pressure Variations Induced by the Tornado Generator

The guide vanes of the tornado generator could have aerodynamic effects on the train even without the vortex air flow. We performed two numerical simulations for the train operating with and without the tornado generator. (Actually, the run without the generator is the same one as in Sect. 6.1 and Fig. 14.) Note that there was no air flow through the generator in both simulations.

Figure 15 shows the comparison of pressure variations at points $P_1 - 2$ and $P_1 - 5$ for the two simulations. There are two negative indentations of roughly 20Pa on the pressure curve with the tornado generator, occurring when the train enters and leaves the tornado generator. Although in Fig. 15 the impact of the guide vanes seems to be significant, pressure variations on the train induced by the EF1 tornado-like vortex (see Fig. 18 below) are of order of $500-1500$Pa. In this sense, the influence of the guide

vanes is negligible.
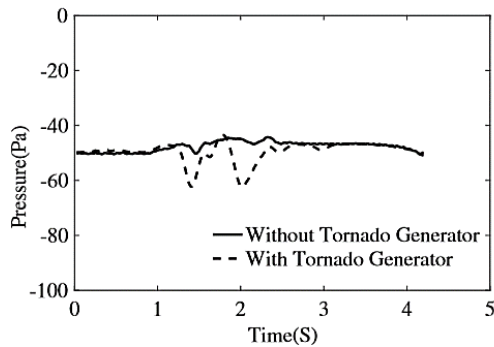


(a) Monitoring point $P_1$-2
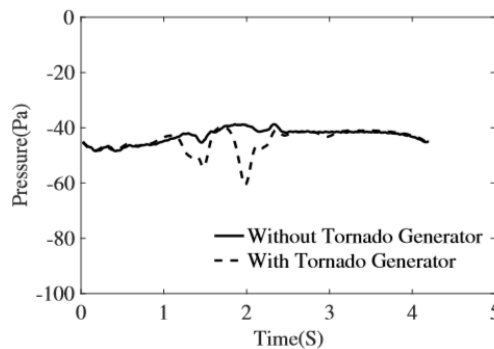


(b) Monitoring point $P_1$-5

**Fig. 15. Comparison of numerical pressure fluctuation at monitoring points with and without tornado generator. Note that the tornado-like vortex is absent in both cases.**

## 7. RESULTS AND ANALYSIS

### 7.1 Effects of the Train on the Tornado-Like Vortex

The train speed, 250km/h, is larger than a characteristic tangential velocity of the vortex corresponding to EF1 tornados. Thus, the air flow induced by the train motion can effect the flow structure of the vortex, although the effect is limited to the vicinity of the train. As shown in Fig. 16, the train moving along the three paths impacts the vortex structure differently.

On $d^+$, the vortex is significantly weakened by the train-induced wind flowing against the rotation of the vortex (panels (a) and (d)). The center of the vortex is slightly pushed away from its original location. For the train running through the vortex center ($d^0$ case), the vortex structure is split into two small vortices by the train head (panel (b)), and destroyed afterwards as the train completely blocks the rotational flow all the way up to the train roof (panel (e)). Different from the other two cases, the vortex is essentially preserved when the train runs along with the rotational flow in the $d^-$ case (panel (c)). The weakening of vortex intensity is caused by the flow blockage of the train body, as well as the interaction of vortex and flow induced by the train motion. One can see from panels (g)-(i) in Fig. 16, that the vortex

is completely destroyed by the wake flow after the train passes through. That the air flow induced by train motion affects the intensity and shifts the center of the tornado-like vortex is consistent with results presented in Suzuki and Okura (2016). The effect varies as the relative position of the train and the vortex changes. Pressure fluctuations are more pronounced for the train moving along $d^-$, which is possibly the most dangerous case.

### 7.2 Pressure Variations on the Train

Once the vortex flow and the pressure distribution are computed, we can turn to the main objective of the paper: the impact of the vortex on the train. When the train is passing through the vortex, the pressure distribution on the train is constantly changing. Figure 17 shows the pressure distribution on the train surface at three instances. The aerodynamic impact of the tornado-like vortex on the train is local. Only the portion of the train within or near the vortex core (about $2.6 - 2.7$m before and past the center line of vortex, see Sect. 5.1) is subjected to a significant negative pressure, while other portions remains as if moving in the open air.

Pressure difference between two sides of the train contributes the most to the lateral force acting on the train. Figure 18 demonstrates the pressure change at monitoring points $P_1 - 2$ and $P_1 - 5$ for $d^+$, $d^0$, and $d^-$ cases. Points $P_1 - 2$ and $P_1 - 5$ are located symmetrically on the left side and the right side of car $C_1$, respectively. The pressure variation patterns of different monitoring points on the same side are similar to each other, as they pass by the vortex center in a sequence.

Generally, the pressure of all the monitoring points is constant before the train enters the vortex, drops rapidly as approaching the center, and restores to the initial state after leaving the vortex. The minimum pressure occurs in the vicinity of the vortex center, but the exact moment of minimum pressure for $P_1 -2$ is a bit later than that for $P_1 -5$. The magnitude of minimum pressure of $P_1 - 5$ decreases from $d^+$ to $d^-$, while that of $P_1 - 2$ increases. For the $d^-$ case, the difference of the minimum pressure between the two monitoring points is significantly larger than that for other cases. The pattern of pressure variations at $P_1 - 2$ and $P_1 - 5$ holds for all other pairs of monitoring points.

### 7.3 Aerodynamic Forces Acting on the Train

The vortex induces significant pressure variations on the train, affecting the aerodynamic loads acting on the train. In this section, we discuss change of the lift, lateral force, and the rolling moment induced by the vortex. These changes determine the operation safety of the train encountering a tornado. The aerodynamic forces are obtained by integrating the pressure and viscous forces over the train surface. The aerodynamic moments $\vec{M}$ are

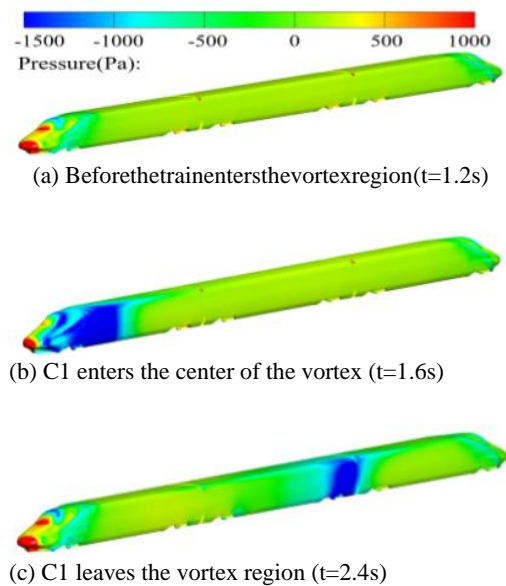$$\vec{M} = \int_{\Sigma} \vec{r} \times (p\vec{n} + \tau\vec{t}) \, d\Sigma \qquad (3)$$

where $\vec{n}$, $\vec{t}$, and $\vec{r}$ are the local unit vector normal to the surface, tangential to the surface, and the corresponding arm, respectively, $p$ is the pressure, $\tau$

Pressure(Pa): -3000  -2500  -2000  -1500  -1000  -500  0  500
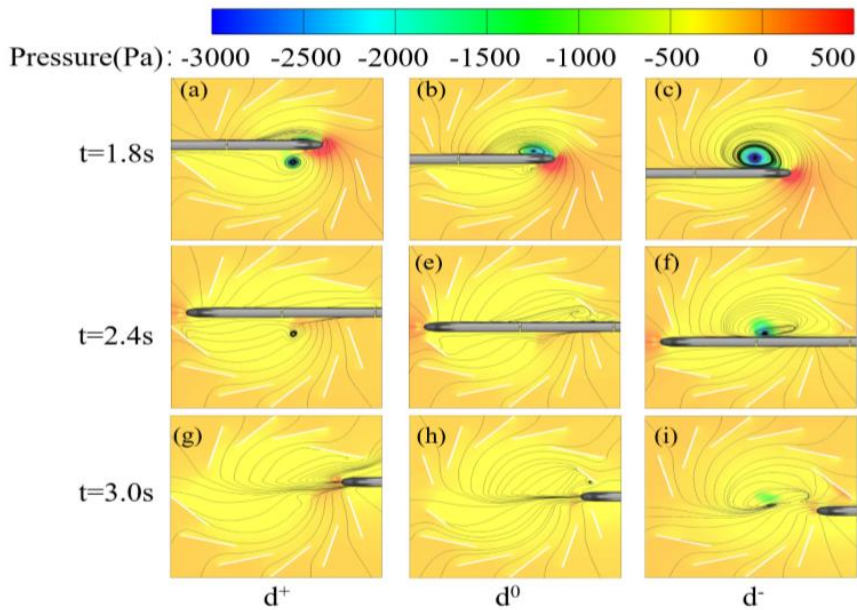


**Fig. 16. Pressure distribution on the horizontal plane 2.28m above the ground for $d^+$ (left column), $d^0$ (center column), and $d^-$ (right column) at t = 1.8s (top row), $t = 2.4$s (middle row), and $t = 3.0s$ (bottom row). Black lines are 2D streamlines at the current flow time. The train is running from left to right.**

is the shear stress tensor, and $\Sigma$ is the area. The rolling moment ($M_x$) of the train is the component of $\vec{M}$ along the direction of train operation, which is the x-axis in the current study. Conventionally, the center of the rolling moment is at the lowest point of the wheel on the side of the lower pressure. Let us introduce dimensionless forces and moments:

$$C_y = \frac{F_y}{1/2\rho V^2 S} \qquad C_{mx} = \frac{M_x}{1/2\rho V^2 SH} \quad C_z = \frac{F_z}{1/2\rho V^2 S}$$
(4)

-1500  -1000  -500  0  500  1000
Pressure(Pa):



(a) Before the train enters the vortex region (t=1.2s)



(b) C1 enters the center of the vortex (t=1.6s)



(c) C1 leaves the vortex region (t=2.4s)

**Fig. 17. Pressure distribution on the train for d$^-$ case at different moments. The train is running from right to left. Low pressure regions (blue) are where the tornado-like vortex is.**

Here coefficients $C_z$, $C_y$, and $C_{mx}$ are normalized lift $F_z$, lateral force $F_y$, and rolling moment $M_x$ acting on the train, respectively. The density of air, $\rho$, remains constant during simulations. V = 250km/h is the speed of the train. S = 11.22m$^2$ and $H = 3.5$m are the area as projected on the $y - z$ plane and the height of the train, respectively.

The gravitational force prevents the train from over-turning. A positive lift reduces the effective weight and increases the risk of overturning. Figure 19 shows the variation of the lift acting on the head car. The lift variations of the other two cars are similar, but with smaller magnitudes. The pressure difference between the top and bottom of the train are main contribute to the lift, and the change of pressure at the top is more pronounced, as the top is directly exposed to the vortex flow. As the vertical tube of negative pressure is located in the center of the generator, the maximum magnitude of the lift occurs on d$^0$ when $C_1$ passes through the vortex center. The lift changes from positive to negative value when the train leaves the core region of the vortex. This phenomenon is more pronounced for d$^-$, because the intensity of the vortex is stronger (see Fig. 16 for details).

The aerodynamic lateral force acting on the train dominates the rolling moment and is a key factor for the safety of the train. Figure 20 presents the lateral force and rolling moment on each car of the train. Overall, the lateral force drops to the minimum values (arrow B in panel (a)) as the train approaches the vortex center, and rise rapidly to the maximum (arrow A in panel (a)) behind the vortex. The rolling moment is essentially a negative of the lateral force. This pattern is consistent with the theoretical study in Baker and Sterling (2018a). The change of sign in the rolling moment causes a swing of the train body,

which compromises the comfort of passengers. The lateral force is a combination of the shear force and the pressure on the train surface, and the pressure force dominates. Thus, variations in the lateral force, and consequently in the rolling moment, are induced mostly by the pressure difference between the two sides of the train. As discussed Sect. 7, there are two causes of the swing of the lateral force and thus of the rolling moment: (i) the pressure on the left side of the train reaches the minimum slightly later than that on the right side,(ii) the magnitudes of the minimum pressure on the left and right sides are different.



(a) $d^+$



(b) $d^0$
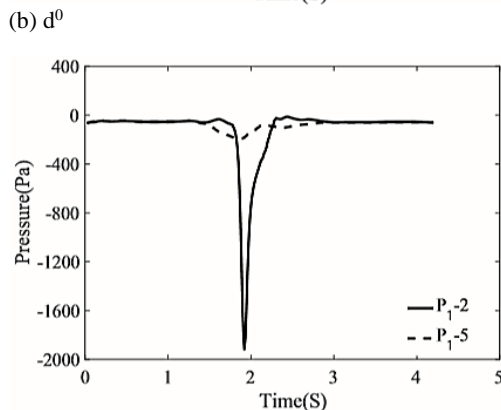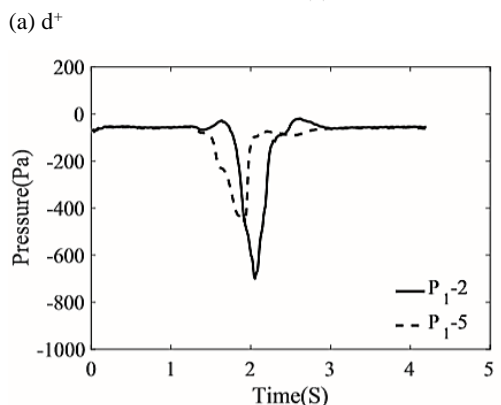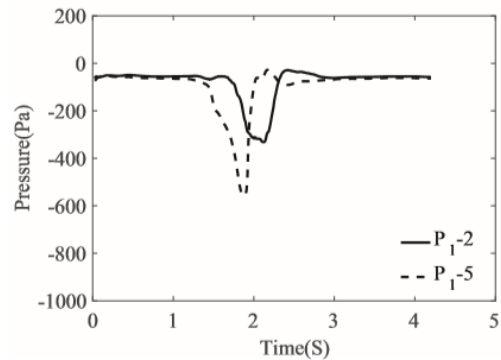


(c) $d^-$

**Fig. 18. Pressure variation of monitoring points $P_1 - 2$ and $P_1 - 5$. Note that the scale of y axis is different for panel (c).**

In terms of the operational safety, it is the maximum absolute value of the rolling moment on the train that matters most, rather than the difference between the maximum and minimum values. The rolling moment

acting on the head car $C_1$ is roughly the same for $d^0$ and $d^-$, while that along $C_2$ and $C_3$ is significantly larger along $d^-$ than along the others. In this sense, the train is subjected to the largest aerodynamic rolling moment in the scenario of $d^-$ overall.
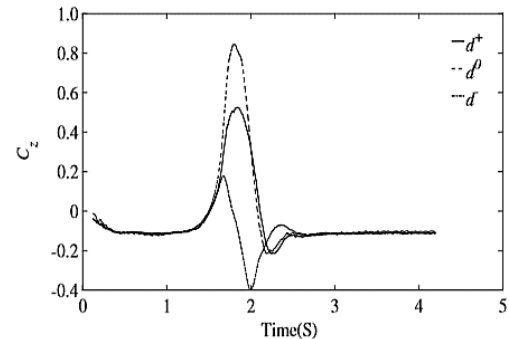


**Fig. 19. Variation of the lift force on $C_1$.**

## 8. DISCUSSION

The tornado-like vortex in the current study is stationary. However, tornadoes in real life are moving along random paths, whose moving speed can range from nearly stationary to more than 100km/h. A typical tornado travels at $10 - 30$km/h NOAA (2018). Comparing to typical tornadoes, the speed of the high-speed train considered herein (250km/h) is much faster than that of the tornadoes. In this sense, it is reasonable to assume that the tornado is stationary as mentioned in Li *et al.* (2019c).

Numerical simulations show that the maximum lift force and rolling moment acting on the train are roughly 28kN and 110kN · m, respectively, and occur to the head car ($C_1$) when the train runs along the $d^-$ path. Gravity is the only force that prevents the train from overturning. The anti-overturning moment due to gravity is $M_g = mgW/2$, where $m$ and $W$ are the mass and width of each car of the train. A typical weight of each car of the train is 50 tons, and the width is 3.38m, which gives the weight $\approx 490$kN and the anti-overturning moment $\approx 830$kN · m. Thus, comparing to the gravitational force and anti-overturning moment of the train due to gravity, the aerodynamic lift and rolling moment induced by the tornado-like vortex of level EF1 are both relatively small. The tornado-like vortex studied in this paper is not strong enough to overturn the train, but causes a lateral shaking while the train passes through.

## 9. CONCLUSIONS

This paper presents a numerical method for simulating a train passing through a stationary tornado-like vortex. We proposed a numerical tornado generator that allowed us to develop a self-consistent model of a tornado-train interaction on the realistic scale. The sliding mesh approach was verified by a moving model experiment. With the validated computational method, the interaction of the train and vortex was investigated. It was found
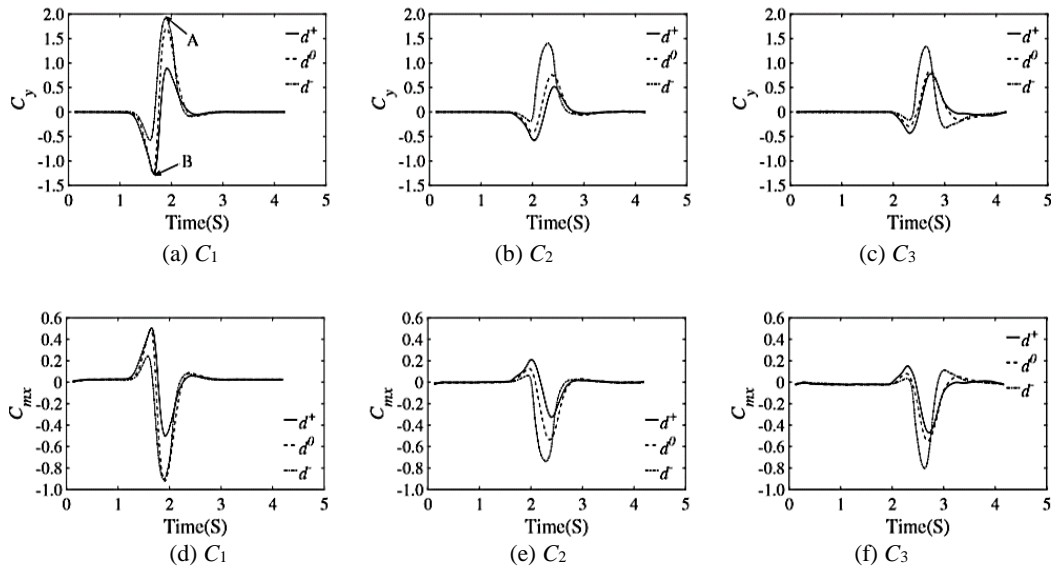
**Fig. 20. Lateral force (upper panels) and rolling moment (lower panels) acting on each car of the train.**

that the train body and the wind induced by the train significantly weakened the intensity of the vortex. However, the weakening effect depended on the path of the train relative to the vortex: it was more significant when the train ran against the swirling flow.

We investigated transient variations of the aerodynamic loads acting on the train, including the lift, lateral force, and rolling moments, which are paramount for the operation safety of train under severe wind conditions. Due to the difference in the magnitudes and the timing of the pressure drop on the left and right side of the train, the tornado-like vortex caused a swing of the lateral force, and consequently, of the rolling moment. We showed that it was more dangerous for the train to pass through the vortex region along the flow rotation, as the strength of the tornado-like vortex was less weakened in this case. The proposed method can be used to assess the operational safety of trains for different strengths of tornados. Different train speeds, as well as different vortex sizes and intensities, will be addressed in subsequent publications.

## ACKNOWLEDGEMENTS

## REFERENCES

Alexander, C. R. and J. Wurman (2004). The 30 may 1998 spencer, south dakota, storm. part i: The structural evolution and environment of the tornadoes. *Monthly Weather Review*133(133), 72–97.

Ashley, W. S. (2007). Spatial and temporal analysis of tornado fatalities in the united states: 1880 2005. *Weather & Forecasting* 22(6),1214-1228.

Baker, C. J. and M. Sterling (2017). Modelling wind fields and debris flight in tornadoes. *Journal of Wind Engineering and Industrial Aerodynamics* 168, 312–321.

Baker, C. J. and M. Sterling (2018a). The calculation of train stability in tornado winds. *Journal of Wind Engineering and Industrial Aerodynamics* 176, 158–165.

Baker, C. J. and M. Sterling (2018b). A conceptual model for wind and debris impact loading of structures due to tornadoes. *Journal of Wind Engineering and Industrial Aerodynamics* 175, 283–291.

Bech, J., M. Gaya, M. Aran, F. Figuerola, J. Amaro and J. Ars (2009). Tornado damage analysis of a forest area using site survey observations, radar data and a simple analytical vortex model. *Atmospheric Research* 93(1), 118–130.

Burgers, J. M. (1948). A mathematical model illustrating the theory of turbulence. *Advances in Applied Mechanics* 1, 171–199.

Charles, A. D. I., H. E. Brooks and N. Dotzek(2009). On the implementation of the enhanced fujita scale in the usa. *Atmospheric Research* 93(1), 554–563.

Chen, Z. W., T. H. Liu, Z. H. Jiang, Z. J. Guo and J. Zhang (2018). Comparative analysis of the effect of different nose lengths on train aerodynamic performance under crosswind. *Journal of Fluids and Structures* 78, 69–85.

Church, C. R., J. T. Snow, G. L. Baker and E. M. Agee (1979). Characteristics of tornado-like vortices as a function of swirl ratio: A laboratory investigation. *Journal of the Atmospheric Sciences* 36(36), 1755–1776.

Eichinger, S., M. Sima, and F. Thiele (2015).

Numerical simulation of a regional train in cross-wind. *The Proceedings of the Institution of Mechanical Engineers, Part F: Journal of Rail and Rapid Transit* 229(6), 625–634.

Haan, F. L., P. P. Sarkar and W. A. Gallus (2008). Design, construction and performance of a large tornado simulator for wind engineering applications. *Engineering Structures* 30(4), 1146–1159.

Haan, F. L., P. P. Sarkar, G. A. Kopp and D. A. Stedman (2017). Critical wind speeds for tornado-induced vehicle movements. *Journal of Wind Engineering and Industrial Aerodynamics* 168, 1–8.

Huang, S., H. Hemida and M. Z. Yang (2014). Numerical calculation of the slipstream generated by a crh2 high-speed train. *The Proceedings of the Institution of Mechanical Engineers, Part F: Journal of Rail and Rapid Transit* 230(1), 103–116.

Ishihara, T., S. Oh and Y. Tokuyama (2011). Numerical study on flow fields of tornado-like vortices using the les turbulence model. *Journal of Wind Engineering and Industrial Aerodynamics* 99(4), 239–248.

Kosiba, K. and J. Wurman (2010). The three-dimensional axisymmetric wind field structure of the spencer, south dakota, 1998 tornado. *Journal of the Atmospheric Sciences* 67(9), 3074–3083.

Li, T., J. Zhang, M. Rashidi and M. Yu (2019a). On the Reynolds-averaged navier-stokes modelling of the flow around a simplified train in crosswinds. *Journal of Applied Fluid Mech*anics 12(2), 551–563.

Li, X. L., F. Wu, T. Yu, M. Z. Yang, N. Robert and V. Dmitri (2019b). Numerical study of the air flow through an air-conditioning unit on high-speed trains. *Journal of Wind Engineering and Industrial Aerodynamics* 187, 26 – 35.

Li, K. M., Y. Xiang, X. L. Hu and H. Y. Qi (2019c). Numerical investigation on temperature and flow characteristics of a tornado-like vortex by using large eddy simulation. *Journal of Applied Fluid Mech*anics 11(3), 585–595.

Li, W., T. H. Liu, J. Zhang, Z. W. Chen, X. D. Chen and T. Z. Xie (2017). Aerodynamic study of two opposing moving trains in a tunnel based on different nose contours. *Journal of Applied Fluid Mech*anics 10(5), 1375–1386.

Liu, T. H., Z. W. Chen, X. S. Zhou and J. Zhang (2017). A cfd analysis of the aerodynamics of a high-speed train passing through a wind-break transition under crosswind. *Engineering Applications of Computational Fluid Mechanics* (1), 1–15.

Liu, Z. Q. and T. Ishihara (2015). Numerical study of turbulent flow fields and the similarity of tornado vortices using large-eddy simulations. *Journal of Wind Engineering and Industrial Aerodynamics* 145, 42–60.

Liu, Z. Q., H. P. Liu and S. Y. Cao (2018a). Numerical study of the structure and dynamics of a tornado at the sub-critical vortex breakdown stage. *Journal of Wind Engineering and Industrial Aerodynamics* 177, 306–326.

Liu, Z. Q., Z. Chong and T. Ishihara (2018b). Numerical study of the wind loads on a cooling tower by a stationary tornado-like vortex through les. *Journal of Fluids and Structures* 81, 656–672.

McDonald, R. James, Kishor and C. Mehta (2006). A recommendation for an enhanced fujita scale (ef-scale). *Wind Science and Engineering Center,* Texas Tech university.

Mishra, A. R., D. L. James and C. W. Letchford (2008). Physical simulation of a single-celled tornado-like vortex, part b: Wind loading on a cubical model. *Journal of Wind Engineering and Industrial Aerodynamics* 96(8), 1258–1273.

Natarajan, D. and H. Hangan (2012). Large eddy simulations of translation and surface roughness effects on tornado-like vortices. *Journal of Wind Engineering and Industrial Aerodynamics* 104-106(104-106), 577–584.

Niu, J., Y. Wang, L. Zhang and Y. Yuan (2018). Numerical analysis of aerodynamic characteristics of high-speed train with different train nose lengths. *International Journal of Heat and Mass Transfer* 127, 188 C 199.

NOAA (2018). *Severe weather 101: Tornados.* National Severe Storms Laboratory.

Paulikas, M. J., T. W. Schmidlin and T. P. Marshall (2016). The stability of passenger vehicles at tornado wind intensities of the enhanced fujita scale. *Weather, Climate, and Society* 8(1), 85 – 91.

Refan, M. and H. Hangan (2016). Characterization of tornado-like flow fields in a new model scale wind testing chamber. *Journal of Wind Engineering and Industrial Aerodynamics* 151, 107–121.

Refan, M. and H. Hangan (2018). Near surface experimental exploration of tornado vortices. *Journal of Wind Engineering and Industrial Aerodynamics* 175, 120–135.

Simmons, K. M. and D. Sutter (2008). Tornado warnings, lead times, and tornado casualties: An empirical investigation. *Weather & Forecasting* 23(2), 246–258.

Suzuki, M. and N. Okura (2016). Study of aerodynamic forces acting on a train using a tornado simulator. *Mechanical Engineering Letters* 2, 00505.

Suzuki, M., K. Obara and N. Okura (2016). An experimental investigation of flow around a vehicle passing through a tornado. *EDP Sciences* 114, 02116.

Suzuki, M., K. Tanemoto and T. Maeda (2003). Aerodynamic characteristics of train/vehicles under cross winds. *Journal of Wind Engineering and Industrial Aerodynamics* 91(1), 209–218.

Tang, Z., C. Feng, L. Wu, D. Zuo and D. L. James (2018). Characteristics of tornado-like vortices simulated in a large-scale ward-type simulator. *Boundary-Layer Meteorology* 166(2), 327–350.

Tari, P. H., R. Gurka and H. Hangan (2010). Experimental investigation of tornado-like vortex dynamics with swirl ratio: The mean and turbulent flow fields. *Journal of Wind Engineering and Industrial Aerodynamics* 98(12), 936–944.

Wang, J., D. Liu, G. Gao, Y. Zhang and J. Zhang (2019). Numerical investigation of the effects of sand collision on the aerodynamic behaviour of a high-speed train subjected to yaw angles. *Journal of Applied Fluid Mechanics* 12(2), 379–389.

Wang, T. T., F. Wu, M. Z. Yang, P. Ji and B. S. Qian (2018). Reduction of pressure transients of high-speed train passing through a tunnel by cross-section increase. *Journal of Wind Engineering and Industrial Aerodynamics* 183, 235 – 242.

Ward, N. B. (1972). The exploration of certain features of tornado dynamics using a laboratory model. *Journal of the Atmospheric Sciences*. 29.

Winn, W. P., S. J. Hunyady and G. D. Aulich (1999). Pressure at the ground in a large tornado. *Journal of Geophysical Research: Atmospheres* 104(D18), 22067–22082.

Wood, V. T. and R. A. Brown (2011). Simulated tornadic vortex signatures of tornado-like vortices having one- and two-celled structures.

*Journal of Applied Meteorology and Climatology* 50(11), 2338–2342.

Wurman, J. and C. R. Alexander (2004). The 30 may 1998 spencer, south dakota, storm. part ii: Comparison of observed damage and radar-derived winds in the tornadoes. *Monthly Weather Review* 133(1), 97–119.

Wurman, J., K. Kosiba and P. Robinson (2013). In situ, doppler radar, and video observations of the interior structure of a tornado and the wind-damage relationship. *Bulletin of the American Meteorological Society* 94(6), 835–846.

Xu, F., Y. Q. Xiao, B. Li and J. P. Ou (2013, 8). CFD numerical simulation of tornado wind field characteristics (In Chinese). *Acta Aerodynamica Sinica*. (3), 350–356,370.

Xue, M., K. Zhao, M. Wang, Z. Li and Y. Zheng (2016). Recent significant torna-does in china. *Advances in Atmospheric Sciences* 33(11), 1209–1217.

Zhang, L., H. Liu, N. Stoll and K. Thurow (2017a). Influence of tunnel aerodynamic effects by slope of equal-transect ring oblique tunnel portal. *Journal of Wind Engineering and Industrial Aerodynamics* 169, 106–116.

Zhang, J., K. He, X. Xiong, J. Wang and G. Gao (2017b). Numerical simulation with a des approach for a high-speed train subjected to the crosswind. *Journal of Applied Fluid Mechanics* 10(5), 1329–1342.

Zhuang, Y. Q. and X. Y. Lu (2015). Numerical investigation on the aerodynamics of a simplified high-speed train under crosswinds. *Theoretical and Applied Mechanics Letters* 5(5), 181–186.